THE JOURNAL OF PHYSICAL CHEMISTRY B
A JOURNAL OF THE AMERICAN CHEMICAL SOCIETY

pubs.acs.org/JPCB

Article

Styrene–Maleic Acid Copolymer Nanodiscs to Determine the Shape of Membrane Proteins

Cheol Jeong, Ryan Franklin, Karen J. Edler, Kenno Vanommeslaeghe, Susan Krueger, and Joseph E. Curtis*

Cite This: *J. Phys. Chem. B* 2022, 126, 1034–1044

Read Online

ACCESS | Metrics & More | Article Recommendations | Supporting Information

ABSTRACT: Lipid nanodiscs can be used to solubilize functional membrane proteins (MPs) in nativelike environments. Thus, they are promising reagents that have been proven useful to characterize MPs. Both protein and non-protein molecular belts have shown promise to maintain the structural integrity of MPs in lipid nanodiscs. Small-angle neutron scattering (SANS) can be used to determine low-resolution structures of proteins in solution, which can be enhanced through the use of contrast variation methods. We present theoretical contrast variation SANS results for protein and styrene–maleic acid copolymer (SMA) belt 1,2-dimyristoyl-*sn*-glycero-3-phosphorylcholine (DMPC) nanodiscs with and without additional bound or transmembrane proteins. The predicted scattering properties are derived from atomistic molecular dynamics simulations to account for conformational fluctuations, and we determine deuterium-labeling conditions such that SANS intensity profiles only include contributions from the scattering of the MP of interest. We propose strategies to tune the neutron scattering length densities (SLDs) of the SMA and DMPC using selective deuterium labeling such that the SLD of the nanodisc becomes homogeneous and its scattering can essentially be eliminated in solvents containing an appropriate amount of D_2O. These finely tuned labeled polymer-based nanodiscs are expected to be useful to extract the size and molecular shape information of MPs using SANS-based contrast variation experiments, and they can be used with MPs of any molecular weight.

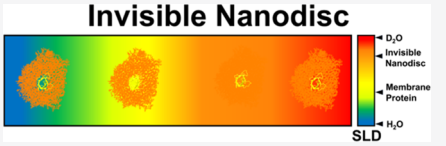

INTRODUCTION

Membrane proteins (MPs) have a diverse set of functions that are essential for life.[1] Despite the progress made in the structural determination of soluble proteins over the past several decades, structural studies of MPs are more challenging due to their inherent physical properties.[2,3] While many strategies have been developed to isolate MPs within defined and relevant environments using polymer vesicles,[4] liposomes,[5] micelles,[6] bicelles,[7] and nanodiscs (NDs),[8,9] there is a need to extend the applicability of methods routinely used to study soluble proteins to MPs.

An increasing number of studies of the structure and function of MPs have been reported using self-assembled lipid NDs[10,11] due to their unique advantages to isolate and purify MP samples[12−16] over other approaches using bicelles or liposomes. The discoidal bilayer structure of NDs is soluble in water due to amphipathic macromolecular "belts" that can wrap around hydrophobic lipid tails and stabilize the structure. Two classes of molecular belts are known to form self-assembled nanoparticles with phospholipids: an annulus of apolipoproteins or their derivatives, so-called membrane scaffold proteins (MSPs),[10] and styrene–maleic acid copolymers (SMAs).[14,15,17,18] The molecular structures of NDs have been investigated by various experimental methods, including nuclear magnetic resonance spectroscopy (NMR),[19−21] cryo-electron microscopy,[22,23] small-angle X-ray scattering (SAXS),[24−27] and small-angle neutron scattering (SANS).[17,24,25] Molecular dynamics (MD) simulations have also provided a valuable insight into the self-assembly of MSP nanodiscs (MSPNDs)[28−32] and SMA nanodiscs (SMANDs).[33]

Small-angle scattering (SAS) using SAXS and/or SANS can be used to obtain low-resolution structural information of soluble proteins. Due to the significantly different neutron scattering properties of hydrogen and deuterium isotopes, SANS is the method of choice for contrast variation experiments where one can isolate the scattering contribution from one component in a multicomponent system.[34] This is accomplished by carrying out a series of measurements of samples with different hydrogen and deuterium content, either in the molecular components themselves and/or in the solvent.

Figure 1 shows a plot of the neutron scattering length density (SLD), a measure of the scattering strength, as a function of the percent of D_2O (% D_2O) in the solvent for several important components of MSPNDs and SMANDs. The difference between the SLD of a ND component and water (black curve) for any given % D_2O is called the contrast. The % D_2O where the SLD of water crosses that of the ND

Received: June 8, 2021
Revised: December 14, 2021
Published: January 28, 2022

https://doi.org/10.1021/acs.jpcb.1c05050
J. Phys. Chem. B 2022, 126, 1034–1044

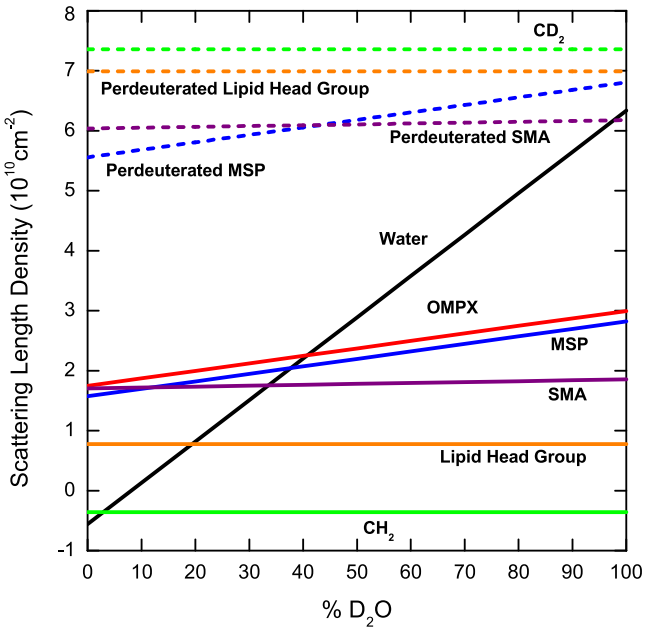

Figure 1. Neutron scattering length density as a function of the % D_2O in the solvent for several important components of MSPNDs and SMANDs.

component of interest is called the contrast match point. For example, the match point of SMA (purple line) is near 30% D_2O. Here, the SLDs of the solvent (water) and SMA are equal, and the SMA does not contribute to the scattering and is essentially invisible or contrast-matched. The match point of perdeuterated SMA (dotted purple line), where all of the H atoms bound to C atoms are replaced with D during synthesis, is closer to 100% D_2O. So, perdeuterated SMA would be visible in a 30% D_2O solvent but not in a 100% D_2O solvent. In the case of MSP (blue line), the match point of perdeuterated MSP (dotted blue line) is above 100% D_2O, and so a lower amount of deuteration would be desirable to contrast match MSPs in 100% D_2O. Thus, the amount of deuteration, also known as deuterium labeling, can be tuned to obtain the desired match point of a given ND component.

The scattering intensity, $I(q)$, is proportional to the square of the sum of the contrasts of the components in the NDs.[34] The intensity is a function of q, which is related to the scattering angle and wavelength of the neutrons.[34] The key factor is to arrange conditions by varying the amount of deuteration in the ND components and the solvent D_2O/H_2O ratio such that there is measurable scattering intensity of one component that dominates the scattering intensity, while the scattering intensity of the other components, on average, matches the solvent scattering so that the other components do not contribute to the scattering intensity. Since only the average contrast of the other components is matched, some q-dependent residual scattering is usually present due to the different SLDs of the individual components.

Several SANS contrast variation studies have demonstrated conditions to study MPs in contrast-matched carriers such as mixed micelles,[35] deuterated isotropic bicelles[36] in a deuterated buffer solution, and selectively deuterium-labeled MSPNDs[37] that leverage contrast variation and SANS. These labeled carrier approaches are an important advance to utilize contrast variation methods as they could allow one to use the same methodology used for the modeling of soluble proteins[38−41] to analyze MP structures. Here, we briefly summarize the methodologies of preparing contrast-matched carriers.

The first is based on reducing the difference of contrast match points between the hydrophilic head and hydrophobic tails (i.e., lipid head group and CH_2/CD_2 in Figure 1) using selectively deuterated detergents.[35,42] The second utilizes commercially available bicelles with deuterated lipids that are contrast-matched in a 100% D_2O buffer solution.[36,43,44] The third, which we aim to expand upon, utilizes "stealth nanodiscs" with selectively labeled lipid head, tail, and MSP components matched in a 100% D_2O solution while keeping a nativelike bilayer environment.[35]

Using stealth nanodiscs, it was found that the forward scattering intensity, $I(q = 0)$, of the 100% D_2O-matched labeled MSPNDs was 150-fold lower than that of nonlabeled MSPNDs in a 100% D_2O solvent. Yet, importantly, there was a nontrivial q-dependency in the experimental SANS intensity profile.[37] This residual intensity from the labeled MSPNDs was assumed to be negligible in the structural analysis of the Ca^{2+}-ATPase ACA8[45] and ABC transporter MsbA[46] MPs in labeled MSPNDs, as $I(0)$ for the labeled MSPNDs was estimated to be smaller than that of the MPs by 1 or 2 orders of magnitude. Thus, the stealth nanodisc approximation can be valid for MPs with a molecular weight greater than or equal to that of MsbA or ACA8. However, it may not work well for smaller MPs of a lower molecular weight, as the $I(0)$ value of the MPs may no longer be orders of magnitude larger than the residual scattering from the MSPNDs. Furthermore, unlike micelles or bicelles, the diameter of MSPNDs is controlled by the length of MSP belts, which will limit the size of MPs to form a complex with the contrast-matched MSPND. Thus, for large MPs, it was proposed[37] to use a 100% D_2O-matched labeled liposome even though it also showed a measurable $I(0)$ under matched conditions.

As noted above, the stealth nanodisc assumption is not valid for MPs for which the forward scattering intensity is comparable to the observed residual intensity of the labeled MSPNDs. In this case, it is suggested to explicitly account for the contribution of the labeled MSPNDs in the modeling of the MP structures[37] or to further reduce the residual nanodisc intensity by refining the level of deuteration of MSPNDs.[47] Even though the labeled stealth MSPND approach is an important advance in structural studies of membrane proteins, its broader application is limited by the target protein size due to the observed nontrivial residual q-dependent intensity of the labeled MSPNDs.

There have been no reports of using contrast-matched SMANDs to study membrane proteins, even though they have been shown to provide a nativelike bilayer environment. Just as for the MSPNDs, the key to preparing contrast-matched SMANDs for contrast variation experiments of membrane proteins is to correctly predict the optimal deuteration conditions for the SMA chains as well as the lipids. Neutron SLDs can be calculated using the chemical composition and stoichiometry of each component to predict the scattering contrast of each component as well as that of the ND. But, the SLD is a function of the mass density or molecular volume,[48] which is nontrivial to estimate for SMA chains assembled in nanodiscs. However, calculating SANS profiles using atomistic coordinates rather than estimating the SLD from the chemical composition negates the need to estimate the molecular volume. Thus, it can be a direct method to perform contrast

https://doi.org/10.1021/acs.jpcb.1c05050
J. Phys. Chem. B 2022, 126, 1034−1044

variation experiments *in silico* and gain insight into complex correlations between components in nanodiscs.

In this paper, we present atomistic molecular simulations that predict the results of contrast variation experiments to obtain membrane protein structural information in both MSPNDs and SMANDs consisting of 1,2-dimyristoyl-*sn*-glycero-3-phosphorylcholine (DMPC) lipids with selectively deuterated MSP, SMA, and lipid. Our models incorporate thermal structural fluctuations of the NDs (MSPNDs and SMANDs) through the use of MD simulations. To this end, we have developed force-field parameters to model SMANDs. Local and large-scale structures of SMANDs were measured from MD trajectories and compared with those from MSPNDs. Then, we evaluated the effect of the residual intensity from the labeled MSPNDs under contrast-matched conditions on the SANS intensity of model ND systems containing MPs. For contrast-matched SMANDs, several labeling strategies have been provided, and calculated SANS intensity profiles of the model systems are shown. Our models include peripheral HIV-1 Gag matrix protein (HIV-1 Gag) and integral outer membrane protein X (OMPX) in MSPNDs and SMANDs. The molecular weights of HIV-1 Gag (14.7 kDa) and OMPX (16.4 kDa) are smaller than that of ACA8 (126 kDa) by an order of magnitude. These systems highlight the potential of using labeled SMANDs and contrast variation to determine scalar parameters, structural arrangement, and shape information of small MPs in model lipid environments. We anticipate that our prediction for contrast-matched SMAND conditions will contribute to the investigation of membrane proteins using SMANDs with less restriction of membrane protein size than that reported in previous studies using MSPNDs.[37,46,47]

COMPUTATIONAL METHODS

Materials. The compositions of MSPNDs and SMANDs are summarized in Table 1. MSPNDs in our simulations contained two MSP1D1 belt proteins[49] and were experimentally shown[50] to form DMPC nanodiscs with a diameter of 98 Å. Note that the number of lipids in the MSPNDs, N_{lipid}, and the ND dimensions, can be varied by the concentration of lipids used during the formation of nanodiscs.[50]

Table 1. Compositions of MSPND and SMAND Used in Simulations

	MSPND	SMAND
belt	MSP1D1	$S_{45}M_{15}$
N_{belt}	2	5
N_{lipid}	158	158

Contrary to MSP1D1, which has a unique amino acid sequence, SMA is an anionic copolymer composed of styrene (S) and maleic acid (M) monomers, and the dimension and structure of SMANDs are affected by many factors, such as total molecular weight, polydispersity, charge interactions, and the molar ratio of S/M.[15,18]

We first chose the M monomer to have a net negative charge assuming neutral pH.[15] Then, a random sequence of 45 S and 15 M monomers was generated to prepare a 6.4 kDa random SMA copolymer with the constraint that maleic acid was not allowed to bond to an adjacent maleic acid monomer.[51,52] The SMA chains used in this work had a sequence of SSMSSSMSMS SMSSSMSMSS MSSMSSMSSM SSMSSSSSMS SSSSMSSSSS MSSSSSMSSS and were capped at the ends with hydrogen atoms. Note that commercial SMA chains with a range of S/M from 3:1 to 1.2 are known to form nanodiscs with a distribution of nanoparticle size.[17,18,21] The remaining molecular parameters, number of SMA chains and lipids in SMANDs, depend on the size of wrapped bilayers[21,53] as well as the added amount of SMA chains in the particular simulation.[54] Thus, the number of DMPC lipids in the SMANDs was set to be identical to that in MSPNDs. Then, five SMA chains were chosen after performing test MD simulations with different numbers of SMA chains. Therefore, the resulting mass ratio of SMA polymer to lipid is 0.33 in this work. Figure 2 illustrates the final configurations of nanodiscs and MP-associated nanodiscs obtained from MD simulations.

Force Fields. All simulations were performed using the CHARMM36 force field.[55] The CHARMM General Force Field (CGenFF 3.0.1) program[56,57] was used to generate CHARMM36 force-field-compatible parameters for the SMA chains. The CGenFF penalty scores for M and S were 10.077 and 5.591, respectively, when SMS and SSS triads were used.

Since the penalty score for M was near the recommended validation threshold of 10,[57] we then performed conformational sampling to obtain the *ab initio* potential energy surface (PES) for the dihedrals of a methyl-capped maleic acid using the Gaussian03 package[58] and the force field toolkit (ffTK)[59] plugin in VMD 1.9.3[60] (Figure S1). The CGenFF PES of maleic acid was in quantitative agreement with the *ab initio* PES using MP2,[61] except for the energy barrier conformation. MD simulations of the SMANDs were performed using the CGenFF parameters as the first simulation study. Force-field parameterization of the SMA polymers was carried out in ffTK using HF/6-31G++. Allowed styrene and maleic acid-containing triad residues were used (SMS, MSM, SSM, MSS, and SSS) to define patches to combine residues and handle chain termination. These topology definitions were used to generate the random sequence of SMA copolymers, as described in the Materials section.

MD Simulations. MD simulations were conducted using NAMD[62] at 300 K and 1 atm with [NaCl] = 0.2 M. The TIP3P water model[63] was used along with periodic boundary conditions. Preparing initial configurations for solvated MSPNDs and SMANDs started from making a cylindrical shape DMPC bilayer composed of 158 lipids by truncating a fully equilibrated planar DMPC bilayer with an average area per lipid = 62.5 Å^2, which is close to the experimental value of 60 Å^2 at 300 K,[64−66] that had undergone a 10 ns constant pressure−temperature (NPT) simulation. The trimmed bilayer was equilibrated in an implicit solvent under cylindrical boundary conditions, as it was to be inserted into the center of MSPD1 belts. For SMANDs, four to six SMA chains with an extended configuration were initially located around the trimmed bilayer. Under cylindrical boundary conditions, we performed a MD simulation for 100 ps to allow the SMA chains to wrap around the bilayer lipids. Five SMA chains were found to be adequate to wrap the lipid tails within the ND annulus. Thus, our SMAND system has a minimal amount of SMA chains needed to make a model SMAND. The MSPND and SMAND were solvated and ionized in water boxes and energy-minimized for 10 000 steps.

We performed NPT MD simulations using the energy-minimized configurations of the MSPND and SMAND in water boxes for 160 ns. Equilibration of nanodisc structures was monitored by the time trajectories of the radius of gyration

https://doi.org/10.1021/acs.jpcb.1c05050
J. Phys. Chem. B 2022, 126, 1034−1044

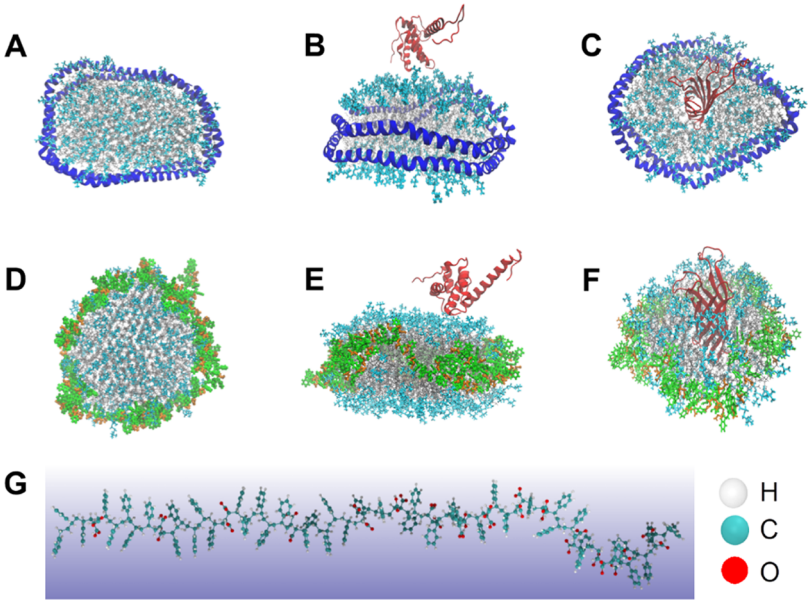

Figure 2. Nanodiscs simulated in this study. (A) MSPND, (B) HIV-1 Gag/MSPND, (C) OMPX/MSPND, (D) SMAND, (E) HIV-1 Gag/SMAND, and (F) OMPX/SMAND. Styrene monomers are represented in green, maleic acids in orange, lipid tails in gray, lipid head groups (choline + glycerol) in cyan, MSPD1 belt protein chains in blue, and membrane proteins (OMPX and HIV-1 Gag) are in red. Waters and ions are not shown. All snapshots are taken from MD trajectories after 160 ns. (G) Energy-minimized configuration of a SMA chain ($S_{45}M_{15}$), where M and S stand for maleic acid and styrene monomers, respectively.

R_g, area per lipid (APL), and bilayer thickness, $h_{bilayer}$, as shown in Figure S2. The equilibration of the nanodisc systems was also monitored by evaluating the SAXS profiles calculated using the SasCalc module in SASSIE-Web[38] (see Figures S3 and S4) and total energy and temperature (see Figures S9 and S10). We used the last 100 ns from the trajectories to evaluate time-averaged structural properties and SAS profiles for the MSPND and SMAND.

Final configurations for the MSPND and SMAND were used to generate the initial configurations for the membrane protein−nanodisc (MP-ND) systems. HIV-1 Gag was placed on the surface of the nanodiscs, while OMPX was placed into the nanodiscs after removing 39 DMPC molecules, as shown in Figure 2. The MP-ND systems were solvated and ionized in water boxes and then energy-minimized. NPT simulations for 80 ns were run, and the last 40 ns from the trajectories were used for data analysis.

Deuterium Labeling of Nanodiscs and Contrast Variation. Deuterium labeling and SANS intensity profile calculations were performed using the SasCalc module in SASSIE-Web[38,67−69] utilizing the MD trajectories. SasCalc allows separate control of the fraction of deuterated nonexchangeable H atoms bonded to carbon atoms, f_{H-D}, and exchangeable H atoms, $f_{exchangeable}$, for each selected group of atoms, which enables random labeling of the lipid head groups including choline and glycerol, alkyl tails, and protein belts independently. $f_{exchangeable}$ was fixed to 0.95, while f_{H-D} was controlled to change the deuteration level for each component.

SANS intensity profiles for the membrane protein contribution, $I_{MP}(q)$, and the nanodisc contribution, $I_{ND}(q)$, were decoupled from the total scattering intensity of the MP-ND systems, $I_{total}(q)$, to analyze the SANS profiles of the MP-NDs and their MP and ND components separately under various D_2O concentration as well as to determine contrast match points. In each case, the scattering intensities calculated by SasCalc were scaled assuming a molar concentration of 0.1 mM. This concentration was chosen so that the calculated SANS intensities are large enough to be comparable to measurable SANS intensities of nanodiscs in a dilute solution, where there are no interparticle interactions. The contrast match points were determined from the x-intercept of a linear fit to $I(0)^{1/2}$ versus fD_2O[32] and are reported as a function of fD_2O in Figure S5. The validity of the labeling schemes was tested by comparing the total scattering from the MP-ND system to that from MP alone with no nanodisc present using q-dependent residuals, defined as residual [%] = $100 \times (I_{total}(q) - I_{MP}(q))/I_{MP}(q)$.

RESULTS

Segregation of SMA in SMANDs. Since the structures of MSPNDs in various conditions have been studied by both simulation[28−30,32] and experiment,[25,40,41] here we first focus on the local structure of the SMA chain wrapping the DMPC bilayer, as shown in Figure 3. SMA chains were observed to form a beltlike structure that was maintained throughout the simulation, consistent with the core−shell model previously used for SANS data analysis of SMANDs.[17]

The segregation in SMA monomers is shown in Figure 3A in which the interfacial regions, e.g., lipid/SMA and SMA/water, are magnified to show the close contact of the S monomers (orange lines) to the lipid tails (gray beads), while the M monomers (blue lines) preferentially populate at the SMA/water interface. The local interaction between DMPC and SMA can be understood by the pair correlation function, $g(r)$, between atoms in the lipids and atoms in the SMA chains. As shown in Figure 3B, a strong correlation between the lipid tail carbon (C_{tail}) and the phenyl carbon in S (C_{ph}) was observed at r = 4.9 Å, followed by the second correlation peak around 10 Å. $g(r)$ for the pair of C_{tail} and the backbone carbon in S (C_S) exhibited a peak at r = 9.1 Å, with a weak correlation close to the first correlation peak position for the C_{tail}−C_{ph} pair, while

https://doi.org/10.1021/acs.jpcb.1c05050
J. Phys. Chem. B 2022, 126, 1034−1044

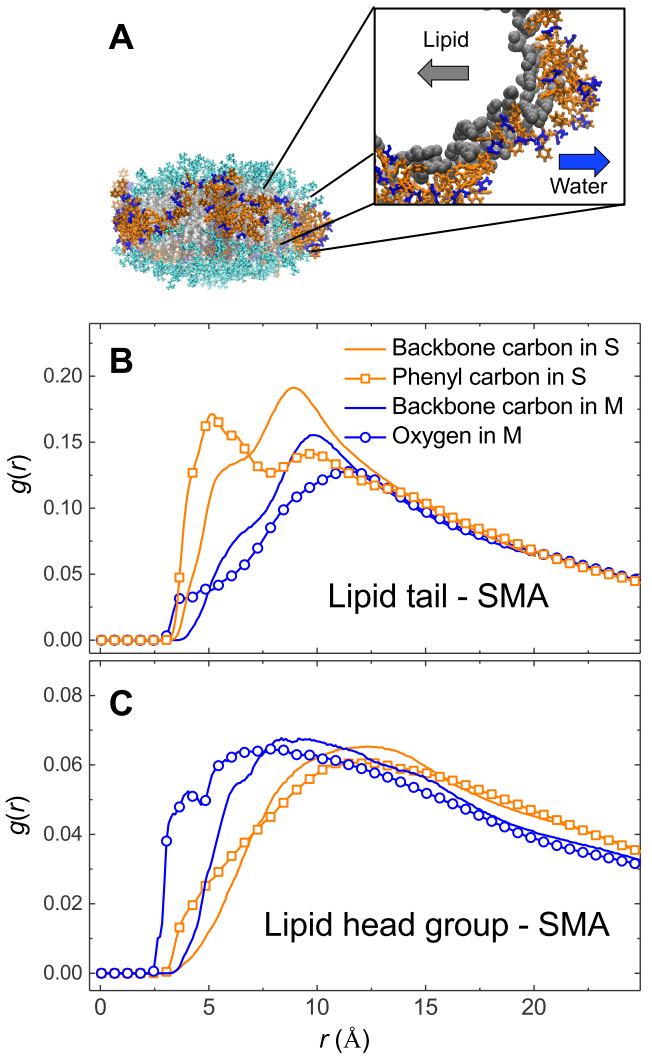

Figure 3. Local correlation of SMA belt chains with the lipid bilayer. (A) Snapshot of the equilibrated SMAND (left) showing the irregular ring shape of the SMA belt (styrene monomers in orange, maleic acid monomers in blue) wrapping around the lipid tail leaflets (carbon in gray) rather than the lipid head groups (cyan). Lipid/SMA and SMA/water interfacial regions (right) are magnified and shown in atomistic detail. Pair correlation functions, $g(r)$, for heavy atom pairs between (B) lipid tails and SMA chains, and between (C) choline groups in the lipids and SMA chains.

the oxygen atom in M (O_M) showed a correlation with C_{tail} at 12 Å.

This observation indicates that the lipid tail/SMA correlation is dominated by C_{tail}−C_{ph} interactions via the hydrophobic portions of the SMA chains. Maleic acid units are segregated from the lipid tail/SMA interface and preferentially located at the SMA/water interface. On the other hand, the lipid head group/SMA correlation, as seen in Figure 3C, was observed to be driven by the interaction between choline and M due to the hydrophilicity of the SMA chain. This hydrophilic nature of SMA has been conjectured to enable the self-assembly of SMANDs in a detergent-free process.[14,15,17]

Dimension and Shape of Nanodiscs. The dimension and shape of MSPNDs and SMANDs were calculated from the simulations using the principal components of the moment of inertia ($I_{11} > I_{22} > I_{33}$) for the lipid bilayer in the nanodiscs and compared to experimental data.[17,50] The shape of the bilayer in the nanodiscs was modeled as an elliptical cylinder, in agreement with the experimental evaluation of the shape of MSPND.[47,70] Three-dimensional parameters for the bilayer in a nanodisc, e.g., two semiaxes (α and β) and $h_{bilayer}$, were determined by eqs S1 and S2 in the Supporting Information. The cylindrical parameters were used to calculate the diameter of the lipid bilayer, $d_{bilayer}$, and APL, as well as the shape anisotropy parameter, $\kappa = \alpha/\beta$, as shown in eq S3 in the Supporting Information, to measure the degree of deformation of shape from a circular cylinder ($\kappa = 1$).

The time-averaged bilayer dimensions $\langle d_{bilayer}\rangle$ and $\langle h_{bilayer}\rangle$ at 300 K for MSPNDs and SMANDs quantitatively agree with experimental data, as seen in Table 2. Interestingly, $\langle$APL$\rangle$ =

Table 2. Average Dimensions and Shapes for MSPNDs and SMANDs from MD Simulations[a]

	MSPND		SMAND	
	sim.	exp.[50,73]	sim.	exp.[17]
$\langle R_{g,ND}\rangle$ [Å]	35.8 ± 0.2		32.7 ± 0.1	
$\langle d_{bilayer}\rangle$ [Å]	76.6 ± 0.4	76[b]	74.2 ± 0.5	76 ± 4
$\langle h_{bilayer}\rangle$ [Å]	45.0 ± 0.4	47[b]	48.0 ± 0.5	46 ± 6
$\langle$APL$\rangle$ [Å^2]	58.4 ± 0.6		54.8 ± 0.7	
$\langle\kappa\rangle$	1.58 ± 0.06		1.10 ± 0.03	

[a] $R_{g,ND}$ is the radius of gyration for the nanodiscs. The dimensions for the lipid bilayer in the nanodiscs, such as the diameter of the lipid bilayer, $d_{bilayer}$, thickness of the lipid bilayer, $h_{bilayer}$, area of the lipid head group per lipid, APL, and the shape anisotropy parameter for the bilayer plane, κ, were calculated from the principal eigenvalues of the moment of inertia tensor, assuming an elliptical cylindrical shape for the lipid bilayer in the nanodisc. κ is defined as a ratio of the longest to the shortest semiaxes for an elliptical object. The expressions for the dimensional parameters for the lipid bilayer as a function of the principal axes parameters are shown in eqs S1−S3. The corresponding experimental data[17,50] for the lipid bilayer dimensions are given for comparison. $\langle$...$\rangle$ is the ensemble-averaged property. [b] Reference data did not contain experimental uncertainties.

58.4 Å^2 from MSPNDs is smaller than the value of 62.5 Å^2 obtained for an infinite bilayer simulated under the same conditions as those of the MSPNDs. This is consistent with previous small-angle scattering,[49,71] MD simulation,[28] and solid-state NMR results showing enhanced lipid order parameters,[20,72] as well as differential scanning calorimetry reports of increased lipid melting temperature, T_m,[73,74] in MSPNDs. Moreover, $\langle\kappa\rangle$ for MSPNDs of about 1.6 was found to be in line with recent experimental MSPND studies[70,75] of their shape deformation.

The simulated SMANDs in this work showed a smaller $\langle R_g\rangle$ than the simulated MSPNDs by 9% but comparable to $d_{bilayer}$ and $h_{bilayer}$ from the SANS experiment.[17] This $\langle R_g\rangle$ reduction for the SMANDs is related to the smaller $\langle d_{bilayer}\rangle$ and $\langle$APL$\rangle$ values compared with the MSPNDs. In our simulations, the bilayer in the SMANDs was observed to maintain the initial circular cylindrical shape as shown by $\langle\kappa\rangle$ about 1.1. Just as for the MSPNDs, the reduction of $\langle$APL$\rangle$ for our model SMANDs may indicate an increase of T_m. Indeed, T_m was experimentally observed to nonmonotonically vary as a function of the molar ratio of SMA to lipid and show a broad T_m distribution.[76] Overall, the size and shape of our model MSPND and SMAND are comparable to experimental results.

SANS Profiles for MPs in Contrast-Matched MSPNDs. Before investigating the properties of labeled MP-ND systems,

https://doi.org/10.1021/acs.jpcb.1c05050
J. Phys. Chem. B 2022, 126, 1034−1044

we compared theoretical SANS profiles for MP-ND systems without labeling the ND components. As shown in Figure S5, calculated SANS intensities, $I_{total}(q)$, for nonlabeled MP-ND systems at the nanodisc match point condition strongly deviate from that for the MP alone, $I_{MP}(q)$, at the same contrast for q values greater than 0.01 Å^{-1}. This deviation of $I_{total}(q)$ from $I_{MP}(q)$ is due to the difference in the contrast match points between lipid head (choline + glycerol), lipid tail, and belt regions of the NDs. The contrast-matched carrier approaches were basically aimed at reducing such a difference in scattering contrasts within these structural components of the NDs. This is explored further for SMANDS in Figure S6, where it is shown that the nonuniform neutron SLDs of the lipid head and tail groups (see Figure 1) prevent the scattering from the NDs from being matched out without selective deuterium labeling.

Figure 4 shows the effect of selectively labeled MSPNDs on the contrast variation of MP-MSPND systems with the small-molecular-weight proteins, HIV-1 Gag and OMPX. In this case, the f_{H-D} for the MSP, lipid head groups, and lipid tail groups was chosen to be 0.70, 0.78, and 0.93, respectively. These f_{H-D} values were taken from those used in the previous stealth MSPND study.[37] The calculated total SANS intensity, $I_{total}(q)$, for the MP-MSPNDs in 100% D_2O was compared to those of the nanodisc, $I_{ND}(q)$, and membrane protein, $I_{MP}(q)$, alone under the same contrast condition.

For both MP-MSPND systems, the calculated $I_{ND}(0)$ values as a function of % D_2O in the solvent were in good agreement with previous experimental data.[37,46] For HIV-1 Gag-MSPNDs, the calculated $I_{MP}(0)$ was about seven times greater than $I_{ND}(0)$, as shown in Figure 4A. The residual plot shows that $I_{total}(0)$ deviates from $I_{MP}(0)$ by 88%. There is also a significant deviation around q = 0.1 Å^{-1}. $I_{total}(q)$ and $I_{MP}(q)$ should be equal under ideal conditions where the SANS intensity from the MSPND is completely matched in 100% D_2O. Therefore, the approximation of stealth MSPNDs is not applicable for the HIV-1 Gag-MSPND system, with an HIV-1 Gag molecular weight of 14.7 kDa, consistent with the previous MSPND study.[37]

A similar deviation of $I_{total}(q)$ from $I_{MP}(q)$ was observed for the OMPX-MSPND system, as shown in Figure 4B. In addition, we also observed that $I_{ND}(q)$ was different from that obtained from the HIV-1 Gag-MSPND system. This variation of $I_{ND}(q)$ between the HIV-Gag and OMPX-MSPND systems resulted from the shape change of the MSPND upon insertion of OMPX into the lipid bilayer. Since HIV-1 Gag is a peripheral membrane protein, no such shape change of the MSPND occurred.

Toward More Complete Contrast-Matched MSPNDs. Our calculations show that further reduction of the residual intensity for MSPNDs is necessary for small-molecular-weight MP characterization. Refined labeling conditions for MSPND were formulated based on Figure 5, which shows the contrast match points in terms of fD_2O as a function of the fraction of nonexchangeable H atoms bonded to C atoms, f_{H-D}, for the components in OMPX-MSPNDs. The black arrow corresponds to f_{H-D} = 0.73, where the SLDs of the lipid head and lipid tail groups are the same. This is less than 0.78 and 0.93,

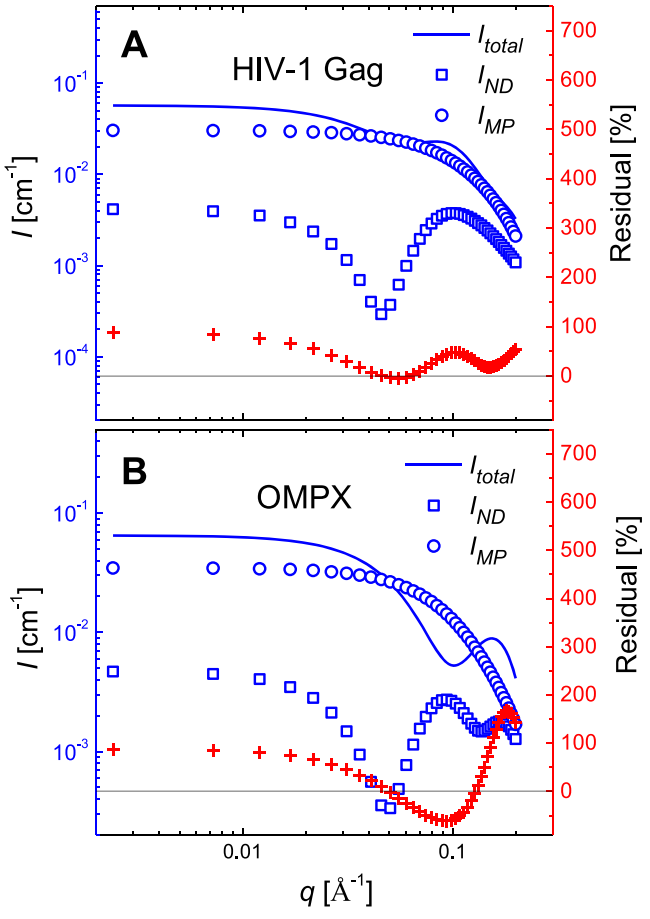

Figure 4. Prediction of SANS profiles in 100% D_2O from MD simulations of (A) HIV-1 Gag-MSPND and (B) OMPX-MSPND in which the deuteration scheme of the previous stealth ND experiment was adopted for our calculation in such a way that nonexchangeable H atoms bonded to C atoms were replaced by D atoms by the ratio of 0.70, 0.78, and 0.93 for the MSP, lipid head (choline + glycerol) groups, and lipid tail groups, respectively. H atoms in the MSP and the lipid tail were randomly selected to be converted to D atoms, while 14 H atoms (nine from three methyl groups and five from glycol) were selectively deuterated among 18 H atoms in the lipid head group. The poor agreement between $I_{total}(q)$ and $I_{MP}(q)$ in both cases indicates that the contribution from $I_{ND}(q)$ is still significant.

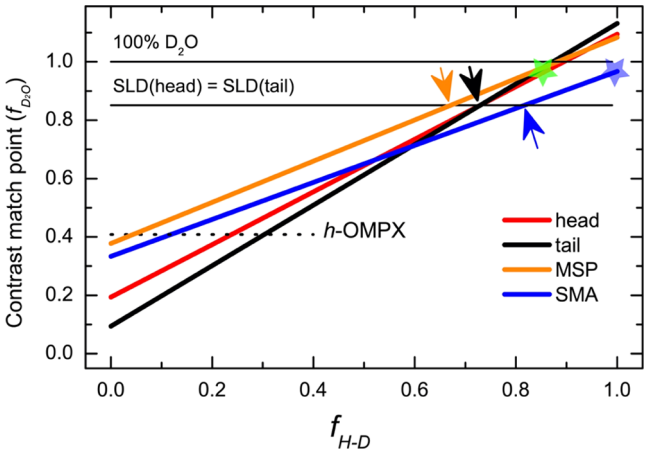

Figure 5. Contrast match points in a fraction of D_2O in the solvent, fD_2O, for the components in OMPX-MSPND and OMPX-SMAND systems as a function of the fraction of deuterated nonexchangeable H atoms bonded to C atoms, f_{H-D}. Equations S4−S7 corresponding to the solid lines can be found in the Supporting Information.

https://doi.org/10.1021/acs.jpcb.1c05050
J. Phys. Chem. B 2022, 126, 1034−1044

Table 3. Composition of Contrast-Matched, Fine-Tuned SMANDs (*f*-SMANDs)

	labeling scheme	f_{H-D} (SMA)	fD_2O
f-SMAND1	D_{random}-PC: f_{H-D} (head) = 0.155; f_{H-D} (tail) = 0.231	0.0	0.334
f-SMAND2	D_{random}-PC: f_{H-D} (head) = 0.730; f_{H-D} (tail) = 0.730	0.817	0.851
f-SMAND3	D_{random}-PC: f_{H-D} (head) = 0.859; f_{H-D} (tail) = 0.842	1.0	0.967

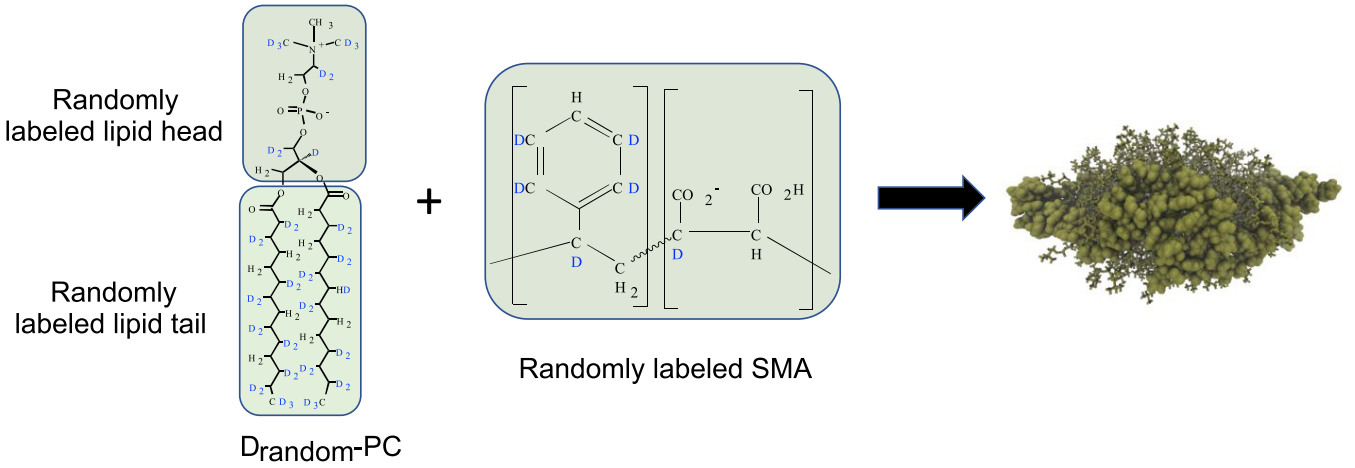

Figure 6. Labeling scheme for contrast-matched SMANDs. Deuterium labeling is treated randomly for the lipid head and tail groups and the SMA chains.

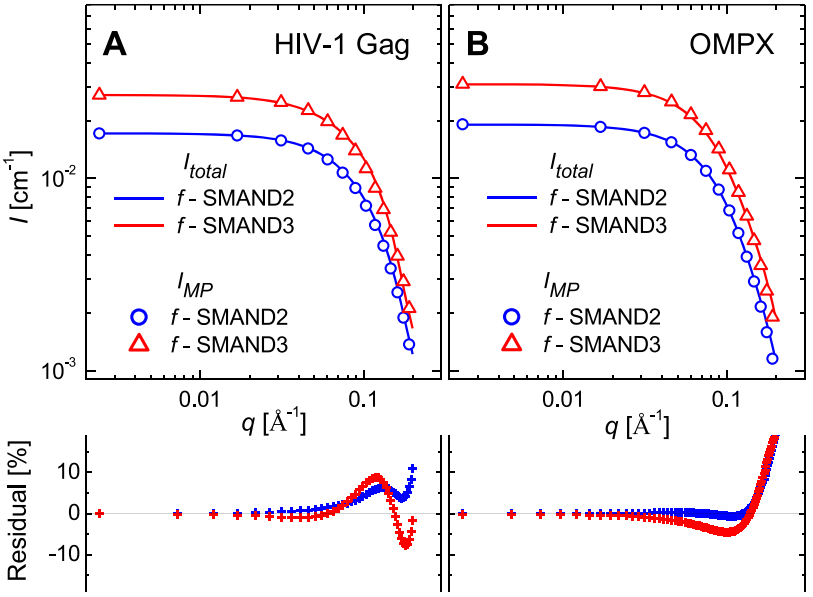

Figure 7. Simulated SANS profiles for fine-tuned SMANDs (*f*-SMANDs) in complex with (A) HIV-1 Gag and (B) OMPX. Lines and symbols indicate the SANS profile for the MP-ND system, $I_{total}(q)$, and for the membrane protein alone, $I_{MP}(q)$, at the corresponding contrast match points for the *f*-SMANDs, respectively. For clarity, only every 6th data point is shown in the SANS profiles, and every 2nd data point is shown in the residual plots.

which are the values used for the lipid head and tail groups, respectively, in the experimental stealth MSPND study.[37] If the MSP could be deuterated to a value of f_{H-D} = 0.67 to achieve the same SLD (orange arrow), the entire MSPND would be contrast-matched in an 85% D_2O solution. This is close to the value of f_{H-D} = 0.70 used in the experimental stealth MSPND study,[37] and so this should be experimentally achievable. The challenging part is to achieve the matching lipid head and tail group SLDs via random deuteration. If this scheme could be implemented experimentally, it should result in better contrast-matched MSPNDs and less residual *q*-dependent scattering. Furthermore, the contrast match point for fully protonated OMPX without deuterium labeling (h-OMPX) is 41% D_2O (dashed line), which is sufficiently different from 85% D_2O for the MSPNDs to allow good data to be obtained for OMPX in contrast-matched MSPNDs.

Another option would be to find deuteration conditions for the MSP, lipid head groups, and lipid tails where all three components are contrast-matched in a 100% D_2O solution. This is desirable due to the lower incoherent background in 100% D_2O as well as the larger difference in contrast match points between h-OMPX and the contrast-matched MSPNDs.

https://doi.org/10.1021/acs.jpcb.1c05050
J. Phys. Chem. B 2022, 126, 1034−1044

The green star in Figure 5 highlights the condition where all three lines approximately cross each other. Here, all three components would be contrast-matched at $f_{H-D} \approx 0.85$ in a 95−97% D_2O solution.

Toward Contrast-Matched SMANDs. Based on the calculation of contrast match points, as shown in Figure 5, Table 3 shows three examples of deuterium-labeling conditions for contrast fine-tuned SMANDs (*f*-SMANDS). f_{H-D} values are summarized depending upon f_{H-D} for the SMA. These *f*-SMANDS are designed to be contrast-matched using random labeling of the lipid head and tail groups as well as the SMA belts, as illustrated in Figure 6. *f*-SMAND1 is composed of fully protonated SMA chains. *f*-SMAND2 represents a nanodisc where the contrast match points for the lipid head group and the lipid tails are identical at the same f_{H-D}. *f*-SMAND3 is made of fully deuterated SMA chains. The *f*-SMANDS are described in more detail below.

f-SMAND1 is a nanodisc for which the SMA belt chains are fully protonated and contrast-matched in a 33% D_2O solution. This can be seen in Figure 1, where the SLD of water (black line) crosses that of SMA (solid purple line). The lipid bilayers are partially labeled such that *f*-SMAND1 would be contrast-matched in a 33% D_2O solution. This condition would be appropriate only for the study of deuterated membrane proteins since the difference in the contrast match point between nonlabeled MPs (such as h-OMPX in Figure 5) and SMAND1 is too small to obtain good data on the MPs, especially since the incoherent background is high under this condition. Deuterated integral membrane proteins are generally difficult to obtain in practice.

f-SMAND2 is a hypothetical nanodisc motivated by our calculations that the lipid head and tail groups showed an identical contrast match point at $f_{H-D} = 0.73$ (black arrow in Figure 5). *f*-SMAND2 was predicted to be contrast-matched in an 85% D_2O solution if $f_{H-D} = 0.82$ for the SMA (blue arrow in Figure 5). *f*-SMAND3 uses perdeuterated SMA chains (blue star in Figure 5) that are contrast-matched in a 97% D_2O solution. This match point can also be observed in Figure 1, where the SLD of water (black line) crosses that of perdeuterated SMA (dashed purple line). f_{H-D} for the lipid head and the lipid tail groups of *f*-SMAND3 were adjusted to the contrast match point of 97% D_2O for the perdeuterated SMA (green star in Figure 5), which corresponds to $f_{H-D} = 0.84$ for the lipid tails and $f_{H-D} = 0.86$ for the lipid head groups.

$I_{total}(q)$ values for contrast-matched *f*-SMAND2 and *f*-SMAND3 were compared with $I_{MP}(q)$ for protonated HIV-1 Gag and OMPX in Figure 7. In each case, the scattering intensities were calculated assuming a total concentration of 0.1 mM. For HIV-1 Gag-*f*-SMANDs, we observed a significant reduction of residuals for the entire q range, as seen in Figure 7A. At most, a 10% deviation of $I_{total}(q)$ from $I_{MP}(q)$ was found for q greater than 0.1 $Å^{-1}$. *f*-SMAND3 is preferred over *f*-SMAND2 due to the ability to synthesize perdeuterated SMA ($f_{H-D} = 1$) that is contrast-matched in 97% D_2O, where there is significantly lower incoherent scattering. The average R_g calculated from a Guinier fit to $I_{total}(q)$ in the range where $q_{max}R_g = 1$ (24 data points) was 16.8 ± 0.3 Å for HIV-1 Gag-*f*-SMAND3 and 16.4 ± 0.1 Å for HIV-1 Gag alone.

f-SMANDs were also contrast-matched in the OMPX-*f*-SMAND system, as shown in Figure 7B, even though OMPX significantly altered the shape of the bilayer in the SMAND. Thus, *f*-SMANDs can be applied in SANS regardless of the membrane protein type. Moreover, using *f*-SMANDs would mitigate the limitation of membrane protein size in contrast to MSPNDs, where the diameter is restricted by the finite circumference of the MSP. Therefore, we expect that using *f*-SMANDs would be a powerful tool in contrast variation SANS experiments for membrane protein characterization, overcoming the limitation of MSPND-based approaches.

Although this paper explores theoretical *f*-SMANDs, three possible formulations of *f*-SMAND3 that can potentially be realized experimentally are explored in Figure S7. For example, $f_{H-D} = 0.84$ for the lipid tails is close to $f_{H-D} = 0.86$ for the lipid head groups. Thus, a mixture of commercially available fully protonated and fully deuterated DMPCs having a molar ratio of 15:85 is one way to make *f*-SMAND3. Alternatively, one can use mixtures of labeled DMPCs with randomly deuterated tail groups and either selectively or randomly deuterated head groups. The latter methods are shown to produce an excellent agreement between $I_{total}(q)$ and $I_{MP}(q)$ for simulated OMPX-*f*-SMAND3 systems.

The prediction of scattering profiles for *f*-SMAND systems was based on MD configurations of a single composition of the SMAND. However, it is noted that our method using MD simulations can be generally applicable to a family of SMANDs with different compositions. Considering the experimental findings of broad size and T_m distributions for SMANDs,[17,76] it may be necessary to perform MD studies on the bilayer phase in the SMAND and corresponding contrast match point perturbations[77] caused by changing the size and composition of the SMAND. The optimum labeling conditions of SMANDs that have a nativelike bilayer environment must be validated and refined along with experimental contrast variation studies on deuterium-labeled SMANDs.

CONCLUSIONS

Lipid nanodiscs are a promising tool to characterize membrane proteins. The contrast variation method using SANS has been used to measure low-resolution structures of soluble protein complexes[34] by employing deuterium labeling. Selective labeling for each component of the nanodisc[37] is essential to effectively contrast match the nanodisc in SANS-based contrast variation experiments, enabling the modeling of the membrane protein structure in a manner similar to that of soluble proteins.[45,46] However, the use of SANS for MP-ND systems has been limited to large-molecular-weight membrane proteins of ca. 130 kDa due to the nontrivial contribution of contrast-matched MSPND to the SANS data of the MP-MSPND system. We performed atomistic molecular dynamics simulations on small-molecular-weight membrane proteins, less than 20 kDa, associated with MSP and SMA DMPC nanodisc systems and studied the neutron contrast matching conditions of labeled MSPNDs and SMANDs. In this work, we presented the conformational properties of model SMANDs for the first time by MD simulations based on CHARMM36-compatible force-field parameters for polymeric SMA chains. Our simulation results on the structure of MSPNDs were in quantitative agreement with experiments[20,49,50,70−75] and simulation studies.[28] In addition, this work presents the first MD simulations of SMANDs. We observed in our simulations the segregation of styrene and maleic acid monomers of the SMA belts near the lipid−belt and the belt−water interface, respectively. Model scattering profiles for MSPNDs that were deuterium-labeled as carried out experimentally[37,45,46] showed that the residual q-dependent scattering intensity significantly

https://doi.org/10.1021/acs.jpcb.1c05050
J. Phys. Chem. B 2022, 126, 1034−1044

contributed to the total scattering intensity of the MP-MSPND system at the MSPND contrast match point. To overcome the limitations of the currently used MSPNDs, we proposed labeling conditions for contrast-matched SMANDs as well as MSPNDs that would be applicable to a small membrane protein system.

In this seminal MD study on SMAND systems, we considered a single composition for the SMAND to investigate the conformational properties and to predict corresponding SANS profiles of MP-SMAND systems after applying deuterium labeling. The conformations of SMANDs made with polymer belts are experimentally known to be affected by pH, ionic strength, temperature, SMA composition, etc.[76,78−80] The complexity due to the polymer chain belts can be also considered in our framework to predict and design conditions for SANS measurements for membrane protein characterization. Appropriately labeled SMANDs should be an important tool to fully realize the potential of contrast matching SANS to study membrane proteins of all sizes with important implications in basic biology and medicine.

■ ASSOCIATED CONTENT

Supporting Information

The Supporting Information is available free of charge at https://pubs.acs.org/doi/10.1021/acs.jpcb.1c05050.

Quantum and classical potential energy surfaces for dihedral angles of a methyl-capped SMA monomer (Figure S1); time-dependent structural properties of membrane scaffold protein (MSP) and styrene−maleic acid copolymer (SMA) nanodiscs (NDs) (Figure S2); time trajectory of SAXS profiles of MSPNDs from the MD trajectory up to t = 160 ns (Figure S3); time trajectory of SAXS profiles of SMANDs from the MD trajectory up to t = 160 ns (Figure S4); contrast variation SANS profiles of membrane protein−nanodisc (MP-ND) systems without deuterium labeling (Figure S5); determination of structural units in SMANDs for selective labeling (Figure S6); effect of the deuterium labeling method on a contrast variation experiment for f-SMAND3 (Figure S7); definition of atom name for styrene and maleic acid monomers (Figure S8); time trajectories of the potential energies $_{Epot}$ for MSPND, HIV-1 Gag/MSPND, OMPX/MSPND, SMAND, HIV-1 Gag/SMAND, and OMPX/SMAND (Figure S9); and time trajectories of temperature T for MSPND, HIV-1 Gag/MSPND, OMPX/MSPND, SMAND, HIV-1 Gag/SMAND, and OMPX/SMAND (Figure S10) (PDF)

■ AUTHOR INFORMATION

Corresponding Author

Joseph E. Curtis − *NIST Center for Neutron Research, National Institute of Standards and Technology, Gaithersburg, Maryland 20899, United States;* orcid.org/0000-0001-5818-295X; Phone: 301-975-3959; Email: joseph.curtis@nist.gov

Authors

Cheol Jeong − *NIST Center for Neutron Research, National Institute of Standards and Technology, Gaithersburg, Maryland 20899, United States; Department of Chemistry, The University of Tennessee, Knoxville, Tennessee 37996-1600, United States*

Ryan Franklin − *NIST Center for Neutron Research, National Institute of Standards and Technology, Gaithersburg, Maryland 20899, United States*

Karen J. Edler − *Department of Chemistry, University of Bath, Claverton Down, Bath BA2 7AY, U.K.;* orcid.org/0000-0001-5822-0127

Kenno Vanommeslaeghe − *Department of Analytical Chemistry, Applied Chemometrics and Molecular Modelling—FABI, Vrije Universiteit Brussel (VUB), 1090 Brussels, Belgium*

Susan Krueger − *NIST Center for Neutron Research, National Institute of Standards and Technology, Gaithersburg, Maryland 20899, United States*

Complete contact information is available at: https://pubs.acs.org/10.1021/acs.jpcb.1c05050

Notes

The authors declare no competing financial interest.

■ ACKNOWLEDGMENTS

This work was supported by a joint EPSRC (EP/K039121/1) and NSF (CHE-1265821, OAC-1740087) grant. Certain commercial equipment, instruments, materials, suppliers, or software are identified in this paper to foster understanding. Such identification does not imply recommendation or endorsement by the National Institute of Standards and Technology, nor does it imply that the materials or equipment identified are necessarily the best available for the purpose.

■ REFERENCES

(1) von Heijne, G. The Membrane Protein Universe: What's out There and Why Bother? *J. Intern. Med.* **2007**, *261*, 543−557.

(2) White, S. Membrane Proteins of Known 3D Structure. https://blanco.biomol.uci.edu/mpstruc/ (accessed April 8, 2021).

(3) Carpenter, E. P.; Beis, K.; Cameron, A. D.; Iwata, S. Overcoming the Challenges of Membrane Protein Crystallography. *Curr. Opin. Struct. Biol.* **2008**, *18*, 581−586.

(4) Christian, D. A.; Cai, S.; Bowen, D. M.; Kim, Y.; Pajerowski, J. D.; Discher, D. E. Polymersome Carriers: From Self-Assembly to SiRNA and Protein Therapeutics. *Eur. J. Pharm. Biopharm.* **2009**, *71*, 463−474.

(5) Antonietti, M.; Förster, S. Vesicles and Liposomes: A Self-Assembly Principle Beyond Lipids. *Adv. Mater.* **2003**, *15*, 1323−1333.

(6) Ostermeier, C.; Michel, H. Crystallization of Membrane Proteins. *Curr. Opin. Struct. Biol.* **1997**, *7*, 697−701.

(7) Dürr, U. H. N.; Soong, R.; Ramamoorthy, A. When Detergent Meets Bilayer: Birth and Coming of Age of Lipid Bicelles. *Prog. Nucl. Magn. Reson. Spectrosc.* **2013**, *69*, 1−22.

(8) Denisov, I. G.; Sligar, S. G. Nanodiscs in Membrane Biochemistry and Biophysics. *Chem. Rev.* **2017**, *117*, 4669−4713.

(9) Lee, S. C.; Khalid, S.; Pollock, N. L.; Knowles, T. J.; Edler, K.; Rothnie, A. J.; R T Thomas, O.; Dafforn, T. R. Encapsulated Membrane Proteins: A Simplified System for Molecular Simulation. *Biochim. Biophys. Acta, Biomembr.* **2016**, *1858*, 2549−2557.

(10) Bayburt, T. H.; Grinkova, Y. V.; Sligar, S. G. Self-Assembly of Discoidal Phospholipid Bilayer Nanoparticles with Membrane Scaffold Proteins. *Nano Lett.* **2002**, *2*, 853−856.

(11) Tonge, S. R.; Tighe, B. J. Responsive Hydrophobically Associating Polymers: A Review of Structure and Properties. *Adv. Drug Delivery Rev.* **2001**, *53*, 109−122.

(12) Schuler, M. A.; Denisov, I. G.; Sligar, S. G. Nanodiscs as a New Tool to Examine Lipid−Protein Interactions. In *Lipid-Protein Interactions*; Kleinschmidt, J. H., Ed.; Methods in Molecular Biology; Humana Press: Totowa, NJ, 2013; Vol. *974*, pp 415−433.

(13) Denisov, I. G.; Sligar, S. G. Nanodiscs for Structural and Functional Studies of Membrane Proteins. *Nat. Struct. Mol. Biol.* **2016**, *23*, 481−486.
(14) Knowles, T. J.; Finka, R.; Smith, C.; Lin, Y.-P.; Dafforn, T.; Overduin, M. Membrane Proteins Solubilized Intact in Lipid Containing Nanoparticles Bounded by Styrene Maleic Acid Copolymer. *J. Am. Chem. Soc.* **2009**, *131*, 7484−7485.
(15) Dörr, J. M.; Scheidelaar, S.; Koorengevel, M. C.; Dominguez, J. J.; Schäfer, M.; van Walree, C. A.; Killian, J. A. The Styrene−Maleic Acid Copolymer: A Versatile Tool in Membrane Research. *Eur. Biophys. J.* **2016**, *45*, 3−21.
(16) Lee, S. C.; Pollock, N. L. Membrane Proteins: Is the Future Disc Shaped? *Biochem. Soc. Trans.* **2016**, *44*, 1011−1018.
(17) Jamshad, M.; Grimard, V.; Idini, I.; Knowles, T. J.; Dowle, M. R.; Schofield, N.; Sridhar, P.; Lin, Y.; Finka, R.; Wheatley, M.; Thomas, O. R. T.; Palmer, R. E.; Overduin, M.; Govaerts, C.; Ruysschaert, J.-M.; Edler, K. J.; Dafforn, T. R. Structural Analysis of a Nanoparticle Containing a Lipid Bilayer Used for Detergent-Free Extraction of Membrane Proteins. *Nano Res.* **2015**, *8*, 774−789.
(18) Ravula, T.; Hardin, N. Z.; Ramamoorthy, A. Polymer Nanodiscs: Advantages and Limitations. *Chem. Phys. Lipids* **2019**, *219*, 45−49.
(19) Hagn, F.; Etzkorn, M.; Raschle, T.; Wagner, G. Optimized Phospholipid Bilayer Nanodiscs Facilitate High-Resolution Structure Determination of Membrane Proteins. *J. Am. Chem. Soc.* **2013**, *135*, 1919−1925.
(20) Martinez, D.; Decossas, M.; Kowal, J.; Frey, L.; Stahlberg, H.; Dufourc, E. J.; Riek, R.; Habenstein, B.; Bibow, S.; Loquet, A. Lipid Internal Dynamics Probed in Nanodiscs. *ChemPhysChem* **2017**, *18*, 2651−2657.
(21) Vargas, C.; Arenas, R. C.; Frotscher, E.; Keller, S. Nanoparticle Self-Assembly in Mixtures of Phospholipids with Styrene/Maleic Acid Copolymers or Fluorinated Surfactants. *Nanoscale* **2015**, *7*, 20685−20696.
(22) Postis, V.; Rawson, S.; Mitchell, J. K.; Lee, S. C.; Parslow, R. A.; Dafforn, T. R.; Baldwin, S. A.; Muench, S. P. The Use of SMALPs as a Novel Membrane Protein Scaffold for Structure Study by Negative Stain Electron Microscopy. *Biochim. Biophys. Acta, Biomembr.* **2015**, *1848*, 496−501.
(23) Efremov, R. G.; Gatsogiannis, C.; Raunser, S. Lipid Nanodiscs as a Tool for High-Resolution Structure Determination of Membrane Proteins by Single-Particle Cryo-EM. In *Methods in Enzymology*; Elsevier, 2017; Vol. *594*, pp 1−30.
(24) Putnam, C. D.; Hammel, M.; Hura, G. L.; Tainer, J. A. X-Ray Solution Scattering (SAXS) Combined with Crystallography and Computation: Defining Accurate Macromolecular Structures, Conformations and Assemblies in Solution. *Q. Rev. Biophys.* **2007**, *40*, 191−285.
(25) Skar-Gislinge, N.; Arleth, L. Small-Angle Scattering from Phospholipid Nanodiscs: Derivation and Refinement of a Molecular Constrained Analytical Model Form Factor. *Phys. Chem. Chem. Phys.* **2011**, *13*, 3161−3170.
(26) Kynde, S. A. R.; Skar-Gislinge, N.; Pedersen, M. C.; Midtgaard, S. R.; Simonsen, J. B.; Schweins, R.; Mortensen, K.; Arleth, L. Small-Angle Scattering Gives Direct Structural Information about a Membrane Protein inside a Lipid Environment. *Acta Crystallogr., Sect. D: Biol. Crystallogr.* **2014**, *70*, 371−383.
(27) Bjørnestad, V. A.; Orwick-Rydmark, M.; Lund, R. Understanding the Structural Pathways for Lipid Nanodisc Formation: How Styrene Maleic Acid Copolymers Induce Membrane Fracture and Disc Formation. *Langmuir* **2021**, *37*, 6178−6188.
(28) Shih, A. Y.; Denisov, I. G.; Phillips, J. C.; Sligar, S. G.; Schulten, K. Molecular Dynamics Simulations of Discoidal Bilayers Assembled from Truncated Human Lipoproteins. *Biophys. J.* **2005**, *88*, 548−556.
(29) Shih, A. Y.; Freddolino, P. L.; Sligar, S. G.; Schulten, K. Disassembly of Nanodiscs with Cholate. *Nano Lett.* **2007**, *7*, 1692−1696.
(30) Shih, A. Y.; Arkhipov, A.; Freddolino, P. L.; Sligar, S. G.; Schulten, K. Assembly of Lipids and Proteins into Lipoprotein Particles. *J. Phys. Chem. B* **2007**, *111*, 11095−11104.
(31) Siuda, I.; Tieleman, D. P. Molecular Models of Nanodiscs. *J. Chem. Theory Comput.* **2015**, *11*, 4923−4932.
(32) Debnath, A.; Schäfer, L. V. Structure and Dynamics of Phospholipid Nanodiscs from All-Atom and Coarse-Grained Simulations. *J. Phys. Chem. B* **2015**, *119*, 6991−7002.
(33) Orekhov, P. S.; Bozdaganyan, M. E.; Voskoboynikova, N.; Mulkidjanian, A. Y.; Steinhoff, H.-J.; Shaitan, K. V. Styrene/Maleic Acid Copolymers Form SMALPs by Pulling Lipid Patches out of the Lipid Bilayer. *Langmuir* **2019**, *35*, 3748−3758.
(34) Krueger, S. Designing and Performing Biological Solution Small-Angle Neutron Scattering Contrast Variation Experiments on Multi-Component Assemblies. In *Biological Small Angle Scattering: Techniques, Strategies and Tips*; Chaudhuri, B.; Muñoz, I. G.; Qian, S.; Urban, V. S., Eds.; Advances in Experimental Medicine and Biology; Springer Singapore: Singapore, 2017; Vol. *1009*, pp 65−85.
(35) Oliver, R. C.; Pingali, S. V.; Urban, V. S. Designing Mixed Detergent Micelles for Uniform Neutron Contrast. *J. Phys. Chem. Lett.* **2017**, *8*, 5041−5046.
(36) Dos Santos Morais, R.; Delalande, O.; Pérez, J.; Mouret, L.; Bondon, A.; Martel, A.; Appavou, M.-S.; Le Rumeur, E.; Hubert, J.-F.; Combet, S. Contrast-Matched Isotropic Bicelles: A Versatile Tool to Specifically Probe the Solution Structure of Peripheral Membrane Proteins Using SANS. *Langmuir* **2017**, *33*, 6572−6580.
(37) Maric, S.; Skar-Gislinge, N.; Midtgaard, S.; Thygesen, M. B.; Schiller, J.; Frielinghaus, H.; Moulin, M.; Haertlein, M.; Forsyth, V. T.; Pomorski, T. G.; Arleth, L. Stealth Carriers for Low-Resolution Structure Determination of Membrane Proteins in Solution. *Acta Crystallogr., Sect. D: Biol. Crystallogr.* **2014**, *70*, 317−328.
(38) Curtis, J. E.; Raghunandan, S.; Nanda, H.; Krueger, S. SASSIE: A Program to Study Intrinsically Disordered Biological Molecules and Macromolecular Ensembles Using Experimental Scattering Restraints. *Comput. Phys. Commun.* **2012**, *183*, 382−389.
(39) Rambo, R. P.; Tainer, J. A. Accurate Assessment of Mass, Models and Resolution by Small-Angle Scattering. *Nature* **2013**, *496*, 477−481.
(40) Skar-Gislinge, N.; Kynde, S. A. R.; Denisov, I. G.; Ye, X.; Lenov, I.; Sligar, S. G.; Arleth, L. Small-Angle Scattering Determination of the Shape and Localization of Human Cytochrome P450 Embedded in a Phospholipid Nanodisc Environment. *Acta Crystallogr., Sect. D: Biol. Crystallogr.* **2015**, *71*, 2412−2421.
(41) Graziano, V.; Miller, L.; Yang, L. Interpretation of Solution Scattering Data from Lipid Nanodiscs. *J. Appl. Crystallogr.* **2018**, *51*, 157−166.
(42) Midtgaard, S. R.; Darwish, T. A.; Pedersen, M. C.; Huda, P.; Larsen, A. H.; Jensen, G. V.; Kynde, S. A. R.; Skar-Gislinge, N.; Nielsen, A. J. Z.; Olesen, C.; Blaise, M.; Dorosz, J. J.; Thorsen, T. S.; Venskutonytė, R.; Krintel, C.; Møller, J. V.; Frielinghaus, H.; Gilbert, E. P.; Martel, A.; Kastrup, J. S.; Jensen, P. E.; Nissen, P.; Arleth, L. Invisible Detergents for Structure Determination of Membrane Proteins by Small-angle Neutron Scattering. *FEBS J.* **2018**, *285*, 357−371.
(43) Dos Santos Morais, R.; Delalande, O.; Pérez, J.; Mias-Lucquin, D.; Lagarrigue, M.; Martel, A.; Molza, A.-E.; Chéron, A.; Raguénès-Nicol, C.; Chenuel, T.; Bondon, A.; Appavou, M.-S.; Le Rumeur, E.; Combet, S.; Hubert, J.-F. Human Dystrophin Structural Changes upon Binding to Anionic Membrane Lipids. *Biophys. J.* **2018**, *115*, 1231−1239.
(44) Koutsioubas, A. Low-Resolution Structure of Detergent-Solubilized Membrane Proteins from Small-Angle Scattering Data. *Biophys. J.* **2017**, *113*, 2373−2382.
(45) Josts, I.; Nitsche, J.; Maric, S.; Mertens, H. D.; Moulin, M.; Haertlein, M.; Prevost, S.; Svergun, D. I.; Busch, S.; Forsyth, V. T.; Tidow, H. Conformational States of ABC Transporter MsbA in a Lipid Environment Investigated by Small-Angle Scattering Using Stealth Carrier Nanodiscs. *Structure* **2018**, *26*, 1072−1079.e4.

https://doi.org/10.1021/acs.jpcb.1c05050
J. Phys. Chem. B 2022, 126, 1034−1044

(46) Nitsche, J.; Josts, I.; Heidemann, J.; Mertens, H. D.; Maric, S.; Moulin, M.; Haertlein, M.; Busch, S.; Forsyth, V. T.; Svergun, D. I.; Uetrecht, C.; Tidow, H. Structural Basis for Activation of Plasma-Membrane Ca 2+ -ATPase by Calmodulin. *Commun. Biol.* **2018**, *1*, No. 206.
(47) Maric, S.; Thygesen, M. B.; Schiller, J.; Marek, M.; Moulin, M.; Haertlein, M.; Forsyth, V. T.; Bogdanov, M.; Dowhan, W.; Arleth, L.; Pomorski, T. G. Biosynthetic Preparation of Selectively Deuterated Phosphatidylcholine in Genetically Modified *Escherichia coli*. *Appl. Microbiol. Biotechnol.* **2015**, *99*, 241−254.
(48) Glinka, C. J. Incoherent Neutron Scattering from Multi-Element Materials. *J. Appl. Crystallogr.* **2011**, *44*, 618−624.
(49) Denisov, I. G.; Grinkova, Y. V.; Lazarides, A. A.; Sligar, S. G. Directed Self-Assembly of Monodisperse Phospholipid Bilayer Nanodiscs with Controlled Size. *J. Am. Chem. Soc.* **2004**, *126*, 3477−3487.
(50) Bayburt, T. H.; Sligar, S. G. Membrane Protein Assembly into Nanodiscs. *FEBS Lett.* **2010**, *584*, 1721−1727.
(51) Hill, D. J. T.; O'Donnell, J. H.; O'Sullivan, P. W. Analysis of the Mechanism of Copolymerization of Styrene and Maleic Anhydride. *Macromolecules* **1985**, *18*, 9−17.
(52) Klumperman, B. Mechanistic Considerations on Styrene−Maleic Anhydride Copolymerization Reactions. *Polym. Chem.* **2010**, *1*, 558.
(53) Radoicic, J.; Park, S. H.; Opella, S. J. Macrodiscs Comprising SMALPs for Oriented Sample Solid-State NMR Spectroscopy of Membrane Proteins. *Biophys. J.* **2018**, *115*, 22−25.
(54) Zhang, R.; Sahu, I. D.; Liu, L.; Osatuke, A.; Comer, R. G.; Dabney-Smith, C.; Lorigan, G. A. Characterizing the Structure of Lipodisq Nanoparticles for Membrane Protein Spectroscopic Studies. *Biochim. Biophys. Acta, Biomembr.* **2015**, *1848*, 329−333.
(55) Klauda, J. B.; Venable, R. M.; Freites, J. A.; O'Connor, J. W.; Tobias, D. J.; Mondragon-Ramirez, C.; Vorobyov, I.; MacKerell, A. D.; Pastor, R. W. Update of the CHARMM All-Atom Additive Force Field for Lipids: Validation on Six Lipid Types. *J. Phys. Chem. B* **2010**, *114*, 7830−7843.
(56) Vanommeslaeghe, K.; Hatcher, E.; Acharya, C.; Kundu, S.; Zhong, S.; Shim, J.; Darian, E.; Guvench, O.; Lopes, P.; Vorobyov, I.; Mackerell, A. D. CHARMM General Force Field: A Force Field for Drug-like Molecules Compatible with the CHARMM All-Atom Additive Biological Force Fields. *J. Comput. Chem.* **2010**, *31*, 671−690.
(57) Vanommeslaeghe, K.; Raman, E. P.; MacKerell, A. D. Automation of the CHARMM General Force Field (CGenFF) II: Assignment of Bonded Parameters and Partial Atomic Charges. *J. Chem. Inf. Model.* **2012**, *52*, 3155−3168.
(58) Frisch, M. J.; Trucks, G. W.; Schlegel, H. B.; Scuseria, G. E.; Robb, M. A.; Cheeseman, J. R.; Scalmani, G.; Barone, V.; Mennucci, B.; Petersson, G. A. *Gaussian 09 C.01*; Gaussian, Inc.: Wallingford, CT, 2009.
(59) Mayne, C. G.; Saam, J.; Schulten, K.; Tajkhorshid, E.; Gumbart, J. C. Rapid Parameterization of Small Molecules Using the Force Field Toolkit. *J. Comput. Chem.* **2013**, *34*, 2757−2770.
(60) Humphrey, W.; et al. VMD: Visual Molecular Dynamics. *J. Mol. Graphics* **1996**, *14*, 33−38.
(61) Frisch, M. J.; Head-Gordon, M.; Pople, J. A. A Direct MP2 Gradient Method. *Chem. Phys. Lett.* **1990**, *166*, 275−280.
(62) Phillips, J. C.; Braun, R.; Wang, W.; Gumbart, J.; Tajkhorshid, E.; Villa, E.; Chipot, C.; Skeel, R. D.; Kalé, L.; Schulten, K. Scalable Molecular Dynamics with NAMD. *J. Comput. Chem.* **2005**, *26*, 1781−1802.
(63) Jorgensen, W. L.; Chandrasekhar, J.; Madura, J. D.; Impey, R. W.; Klein, M. L. Comparison of Simple Potential Functions for Simulating Liquid Water. *J. Chem. Phys.* **1983**, *79*, 926−935.
(64) Petrache, H. I.; Dodd, S. W.; Brown, M. F. Area per Lipid and Acyl Length Distributions in Fluid Phosphatidylcholines Determined by (2)H NMR Spectroscopy. *Biophys. J.* **2000**, *79*, 3172−3192.
(65) Kučerka, N.; Nagle, J. F.; Sachs, J. N.; Feller, S. E.; Pencer, J.; Jackson, A.; Katsaras, J. Lipid Bilayer Structure Determined by the Simultaneous Analysis of Neutron and X-Ray Scattering Data. *Biophys. J.* **2008**, *95*, 2356−2367.
(66) Kučerka, N.; Kiselev, M.; Balgavý, P. Determination of Bilayer Thickness and Lipid Surface Areain Unilamellar Dimyristoylphosphatidylcholine Vesiclesfrom Small-Angle Neutron Scattering Curves: A Comparisonof Evaluation Methods. *Eur. Biophys. J.* **2004**, *33*, 328−334.
(67) Perkins, S. J.; Wright, D. W.; Zhang, H.; Brookes, E. H.; Chen, J.; Irving, T. C.; Krueger, S.; Barlow, D. J.; Edler, K. J.; Scott, D. J.; Terrill, N. J.; King, S. M.; Butler, P. D.; Curtis, J. E. Atomistic Modelling of Scattering Data in the Collaborative Computational Project for Small Angle Scattering (CCP-SAS). *J. Appl. Crystallogr.* **2016**, *49*, 1861−1875.
(68) Brookes, E. H.; Anjum, N.; Curtis, J. E.; Marru, S.; Singh, R.; Pierce, M. The GenApp Framework Integrated with Airavata for Managed Compute Resource Submissions: The GenApp Framework Integrated with Airavata. *Concurrency Comput.: Pract. Exper.* **2015**, *27*, 4292−4303.
(69) Watson, M. C.; Curtis, J. E. Rapid and Accurate Calculation of Small-Angle Scattering Profiles Using the Golden Ratio. *J. Appl. Crystallogr.* **2013**, *46*, 1171−1177.
(70) Skar-Gislinge, N.; Simonsen, J. B.; Mortensen, K.; Feidenhans'l, R.; Sligar, S. G.; Lindberg Møller, B.; Bjørnholm, T.; Arleth, L. Elliptical Structure of Phospholipid Bilayer Nanodiscs Encapsulated by Scaffold Proteins: Casting the Roles of the Lipids and the Protein. *J. Am. Chem. Soc.* **2010**, *132*, 13713−13722.
(71) Nakano, M.; Fukuda, M.; Kudo, T.; Miyazaki, M.; Wada, Y.; Matsuzaki, N.; Endo, H.; Handa, T. Static and Dynamic Properties of Phospholipid Bilayer Nanodiscs. *J. Am. Chem. Soc.* **2009**, *131*, 8308−8312.
(72) Mörs, K.; Roos, C.; Scholz, F.; Wachtveitl, J.; Dötsch, V.; Bernhard, F.; Glaubitz, C. Modified Lipid and Protein Dynamics in Nanodiscs. *Biochim. Biophys. Acta, Biomembr.* **2013**, *1828*, 1222−1229.
(73) Denisov, I. G.; McLean, M. A.; Shaw, A. W.; Grinkova, Y. V.; Sligar, S. G. Thermotropic Phase Transition in Soluble Nanoscale Lipid Bilayers. *J. Phys. Chem. B* **2005**, *109*, 15580−15588.
(74) Shaw, A. W.; McLean, M. A.; Sligar, S. G. Phospholipid Phase Transitions in Homogeneous Nanometer Scale Bilayer Discs. *FEBS Lett.* **2004**, *556*, 260−264.
(75) Skar-Gislinge, N.; Johansen, N. T.; Høiberg-Nielsen, R.; Arleth, L. Comprehensive Study of the Self-Assembly of Phospholipid Nanodiscs: What Determines Their Shape and Stoichiometry? *Langmuir* **2018**, *34*, 12569−12582.
(76) Grethen, A.; Oluwole, A. O.; Danielczak, B.; Vargas, C.; Keller, S. Thermodynamics of Nanodisc Formation Mediated by Styrene/Maleic Acid (2:1) Copolymer. *Sci. Rep.* **2017**, *7*, No. 11517.
(77) Knoll, W.; Ibel, K.; Sackmann, E. Small-Angle Neutron Scattering Study of Lipid Phase Diagrams by the Contrast Variation Method. *Biochemistry* **1981**, *20*, 6379−6383.
(78) Tanaka, M.; Hosotani, A.; Tachibana, Y.; Nakano, M.; Iwasaki, K.; Kawakami, T.; Mukai, T. Preparation and Characterization of Reconstituted Lipid−Synthetic Polymer Discoidal Particles. *Langmuir* **2015**, *31*, 12719−12726.
(79) Scheidelaar, S.; Koorengevel, M. C.; van Walree, C. A.; Dominguez, J. J.; Dörr, J. M.; Killian, J. A. Effect of Polymer Composition and PH on Membrane Solubilization by Styrene-Maleic Acid Copolymers. *Biophys. J.* **2016**, *111*, 1974−1986.
(80) Craig, A. F.; Clark, E. E.; Sahu, I. D.; Zhang, R.; Frantz, N. D.; Al-Abdul-Wahid, M. S.; Dabney-Smith, C.; Konkolewicz, D.; Lorigan, G. A. Tuning the Size of Styrene-Maleic Acid Copolymer-Lipid Nanoparticles (SMALPs) Using RAFT Polymerization for Biophysical Studies. *Biochim. Biophys. Acta, Biomembr.* **2016**, *1858*, 2931−2939.

https://doi.org/10.1021/acs.jpcb.1c05050
J. Phys. Chem. B 2022, 126, 1034−1044